Vectorial vortex generation and phase singularities upon Brewster reflection

René Barczyk,[1,2] Sergey Nechayev,[1,2,*] Muhammad Abdullah Butt,[1,2,3] Gerd Leuchs,[1,2] and Peter Banzer[1,2]

[1]*Max Planck Institute for the Science of Light, Staudtstrasse 2, D-91058 Erlangen, Germany*
[2]*Institute of Optics, Information and Photonics, University Erlangen-Nuremberg, Staudtstrasse 7/B2, D-91058 Erlangen, Germany*
[3]*School in Advanced Optical Technologies, University Erlangen-Nuremberg, Paul-Gordan-Strasse 6, D-91052 Erlangen, Germany*

We experimentally demonstrate the emergence of an azimuthally polarized vectorial vortex beam with a phase singularity upon Brewster reflection of focused circularly polarized light from a dielectric substrate. The effect originates from the polarizing properties of the Fresnel reflection coefficients described in Brewster's law. An astonishing consequence of this effect is that the reflected field's Cartesian components acquire local phase singularities at Brewster's angle. Our observations are crucial for polarization microscopy and open avenues for the generation of exotic states of light based on spin-to-orbit coupling, without the need for sophisticated optical elements.

I. INTRODUCTION

Apart from scalar wave properties like intensity and phase, light also has intrinsic spatial vectorial degrees of freedom, described by its polarization distribution [1]. Recently, there is strongly increasing interest in the generation and characterization of complex polarization states of light [2,3]. Their remarkable properties are of paramount importance for a broad range of applications, such as three-dimensional focus shaping [4], laser-based material processing [5], tight focusing of light [6], and Ångström-scale position sensing [7,8], to name a few.

Akin to mechanical objects, light may also possess angular momentum (AM), composed of orbital and spin parts [9–13]. While spin angular momentum (SAM) is attributed to the vectorial (circular) polarization of light, orbital angular momentum (OAM) is associated with the distribution of the scalar phase of a beam, possessing a helical pattern in its cross section with a singularity of arbitrary integer topological charge ℓ on the beam axis. The study of optical OAM has received considerable attention in the literature [2,14,15], displaying great potential in various disciplines, including optical manipulation [16], quantum information protocols [17], and microscopy [18,19].

The coupling between SAM and OAM of light via spin-orbit interaction (SOI) has been studied extensively in the past (see [15] and references therein), e.g., as a means of controlling the OAM or the direction of propagation of an optical beam by its polarization [12,20–30]. A common route towards mediating SOI involves the use of subwavelength gratings [20,21] or anisotropic inhomogeneous media [23,25,31–35]. Another recent approach is based on the polarizing properties of axicons [36] and Fresnel rhombs [37,38]. It utilizes conical reflectors and prisms, where spin-to-orbital angular momentum conversion originates from phase changes upon

total internal reflection as well as from the spin-redirection geometric phase [39–44]. All of these methods rely on the intrinsic or geometric properties of dedicated optical elements. However, SOI naturally occurs as a consequence of AM conservation upon focusing [12,22,45–47] – an inherent process in microscopy.

In this paper, we report on the emergence of vectorial vortex beams, bearing phase singularities, in a surprisingly elementary cylindrically symmetric experimental configuration. The effect is based on SOI of tightly focused circularly polarized (CP) fields [12,15,22,45], reflected from an unstructured planar dielectric substrate [48–53] at Brewster's angle [54]. Even over 200 years after its first description, research articles dealing with Brewster's angle are still being published [55], reporting on remarkable observations such as enhanced spin Hall effect of light [56,57] and mode conversion upon Brewster reflection [58]. Recently, generation of azimuthally polarized vector beams upon reflection of a linearly polarized Bessel beam, the vectorial angular spectrum of which [59] consists of plane waves impinging on a dielectric interface at Brewster's angle, was theoretically proposed [60]. Here, in the first part of the paper, we experimentally confirm the theoretical predictions made for Bessel beams in [52,60]. We use incident tightly focused homogeneously CP light, the vectorial angular spectrum of which encompasses Brewster's angle. Upon reflection of this beam from a planar dielectric interface, we experimentally obtain at Brewster's angle a vector beam with a polarization and phase vortex. We validate our findings by polarization sensitive measurements of the reflected fields' intensity and phase distribution. We analyze the focusing objective's back focal plane (BFP) in the cylindrical transverse electric (TE) and transverse magnetic (TM) polarization basis and reconstruct a central phase vortex in the azimuthal (TE) component. In the second part of the paper, we study the reflected beam in the Cartesian x and y polarization basis. We predict and experimentally measure the emergence of unexpected phase singularities at Brewster's angle in the reflected light after transmission through a linear analyzer.

*sergey.nechayev@mpl.mpg.de
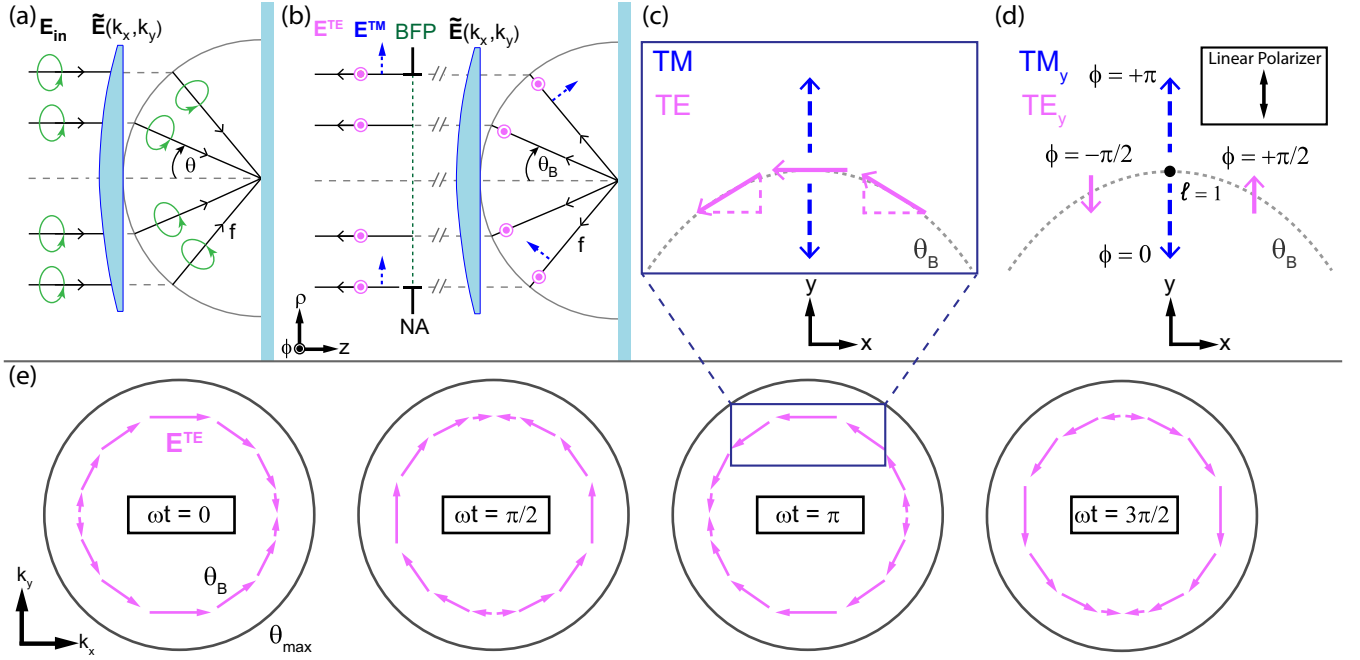
FIG. 1. (a) Focusing scheme of an aplanatic lens for incident circular polarization (CP). The paraxial input field $\mathbf{E}_{in}$ in the back focal plane (BFP) is projected onto a reference sphere of radius f, where the local wave vector is tilted towards the geometrical focus under an angle θ and the CP is preserved for each wave vector. (b) The beam reflected from the substrate is collected by the same objective and analyzed polarization resolved in the BFP. The transverse electric and transverse magnetic (TE and TM) polarized fields E^{TE} and E^{TM} are aligned with the azimuthal and radial cylindrical unit vectors, respectively. For Brewster's angle θ_B, the TM component E^{TM} vanishes. (c) Snapshot in time of CP electric-field components in the reflection BFP around the intersection point of the y axis (origin centered in BFP) and Brewster ring. In contrast to the azimuthal (TE) field, the radial (TM) component exhibits a phase jump of π at θ_B, due to the properties of the Fresnel reflection coefficient r^{TM}. (d) Projection of panel (c) onto the y axis. The projected TE polarized field components on opposite sides of the intersection point possess opposite phase and are inherently $\pm\frac{\pi}{2}$ out of phase with respect to TM in CP light. Consequently, a vortex with topological charge of $\ell = \pm 1$ emerges, with the sign of the phase topological charge depending on the handedness of the incoming polarization state. (e) Time evolution of the polarization distribution in the BFP at Brewster's angle for the reflected vortex beam referred to throughout this paper. Note that for reflection the incident CP field on a ring is multiplied by the corresponding Fresnel reflection coefficient, thus there is no TM polarized field E^{TM} at the ring corresponding to θ_B.

We see two phase singularities appearing at Brewster's angle along the x and y axis for projections of the reflected light in the BFP onto the x and y polarizations, respectively. In consequence, we prove the inevitable presence of polarization and phase vortices for any high numerical aperture (NA) focusing geometry covering Brewster's angle, rendering our observations important especially in the field of polarization microscopy [61–63].

II. THEORY

Consider a Gaussian beam with its waist w_0 coinciding with the BFP of an aplanatic objective with focal length f and NA $= n \sin(\theta_{max})$, where n is the refractive index of the focusing side, and θ_{max} denotes the maximum aperture angle. In this case, the incident field is given by

$$\mathbf{E}_{in} = \underbrace{E_0 \exp\left(-\frac{f^2 \sin^2\theta}{w_0^2}\right)}_{E_{in}} \mathbf{e}_{in}, \quad \theta \leqslant \theta_{max}, \quad (1)$$

with amplitude E_0 and complex polarization vector $\mathbf{e}_{in}$. The spatial extent of the input beam may be characterized by the filling factor $f_0 = w_0/(f \sin \theta_{max})$, i.e., the ratio of beam

waist to objective aperture radius. The lens establishes a link between real-space distribution $\mathbf{E}_{in}(x, y)$ of the paraxial input beam in the BFP and the angular distribution of the focal field $\tilde{\mathbf{E}}(k_x, k_y)$. The transformation it performs may be illustrated by a reference sphere of radius f around the geometrical focus, to which the beam effectively travels undisturbed. A ray impinging on this reference sphere at a distance $\rho = f \sin(\theta)$ from the optical axis is refracted such that it propagates towards the geometrical focus under the divergence angle θ, corresponding to a coordinate transformation of the form [59]

$$(x, y) \rightarrow \left(-f\frac{k_x}{k}, -f\frac{k_y}{k}\right). \quad (2)$$

Here, (x, y) are the BFP Cartesian coordinates, $k = nk_0$ is the wave number of the focusing side, $k_0 = 2\pi/\lambda$ is the free space wave number and λ is the free space wavelength. The process is schematically illustrated for the case of incident CP in Fig. 1(a), whereby upon focusing the polarization is preserved for each wave vector. Since in our case we consider the BFP in reflection, the lens also performs the back-transformation on the reflected field [see Fig. 1(b)]. For deriving the latter, it is convenient to employ the TE and TM polarization basis, with the electric-field vector being orthogonal ($\mathbf{E}^{TE}$) or parallel

($\mathbf{E}^{\mathrm{TM}}$) to the plane of incidence, respectively. In our cylindrically symmetric focusing system, TE and TM are aligned with the azimuthal and radial unit vectors $\mathbf{e}_\phi$ and $\mathbf{e}_\rho$, respectively. Consequently, in this basis, the reflected field $\mathbf{E}_\mathrm{r}$ differs from the incident one only by the factor of the Fresnel reflection coefficients $r^{\mathrm{TE/TM}}$ [59]:

$$\mathbf{E}_\mathrm{r} = \underbrace{\left[r^{\mathrm{TM}}(\theta) \mathrm{E}_{\mathrm{in}}(\mathbf{e}_\rho^* \cdot \mathbf{e}_{\mathrm{in}}) \right] \mathbf{e}_\rho}_{\mathbf{E}^{\mathrm{TM}}} - \underbrace{\left[r^{\mathrm{TE}}(\theta) \mathrm{E}_{\mathrm{in}}(\mathbf{e}_\phi^* \cdot \mathbf{e}_{\mathrm{in}}) \right] \mathbf{e}_\phi}_{\mathbf{E}^{\mathrm{TE}}}, \quad (3)$$

where $*$ denotes the complex conjugate. The minus in Eq. (3) accounts for the fact that we define our cylindrical basis $\{\mathbf{e}_\rho, \mathbf{e}_\phi\}$ with respect to the propagation direction of the incident beam and to the specific form of $r^{\mathrm{TE/TM}}$ given in [59]. Reflection from the surface of a perfect electric conductor ($r_{\mathrm{PEC}}^{\mathrm{TM}} = -r_{\mathrm{PEC}}^{\mathrm{TE}} = 1$) preserves the amplitude and polarization profile of the beam with respect to the fixed laboratory axes (up to a constant phase). In the case of a dielectric interface between media with refractive indices n_1 and n_2, the reflected TM polarized field $\mathbf{E}^{\mathrm{TM}}$ vanishes at Brewster's angle $\theta_B = \arctan(n_2/n_1)$, having peculiar consequences for incident CP light ($\mathbf{e}_{\mathrm{in}} = \mathbf{e}_\pm$), as discussed below.

The polarization unit vectors $\mathbf{e}_\pm$ for CP light may be written as a phase-delayed superposition of Cartesian unit vectors with $\mathbf{e}_\pm \propto (\mathbf{e}_x \pm \iota \mathbf{e}_y)$, where upper and lower signs correspond to left- and right-hand CP light (LCP and RCP), respectively. When switching from the circular ($\mathbf{e}_\pm$) to the cylindrical ($\mathbf{e}_{\rho/\phi}$) basis, the transformation of unit vectors results in an additional phase factor of $\mathbf{e}_\phi^* \cdot \mathbf{e}_\pm \propto \exp(\pm \iota \phi)$ for the azimuthal TE polarized field component (see the Appendix A), i.e., a helical phase profile emerges [22]. In consequence, the reflected TE polarized field $\mathbf{E}^{\mathrm{TE}}$ is an azimuthally polarized vectorial vortex beam with a phase singularity with topological charge of $\ell = \pm 1$ on the optical axis. As mentioned, at θ_B the TM polarized field $\mathbf{E}^{\mathrm{TM}}$ vanishes ($r^{\mathrm{TM}} = 0$) and therefore the purely TE polarized vectorial vortex beam with phase singularity is naturally separated at Brewster's angle. Figure 1(e) schematically depicts the time evolution of the polarization distribution in the BFP for this azimuthal vortex beam, clearly showing the presence of singularities and elucidating the origin of a central phase vortex.

Moreover, analysis typically employed in polarization microscopy consists of a projection of the reflected beam onto the Cartesian polarization basis. Remarkably, this results in two phase vortices with topological charge of $\ell = \pm 1$, emerging at the respective intersection points of Cartesian axis and Brewster ring. The effect originates from the polarizing properties of the Fresnel reflection coefficients and may be understood intuitively by investigating a snapshot in time of the polarization distribution around one of these points [see Fig. 1(c)]. The coefficient r^{TM} exhibits a zero crossing at Brewster's angle, which translates to a phase difference of π for the radial (TM) polarized field below and above θ_B. At the same time, the phase of the azimuthal (TE) component remains unaltered by r^{TE}. Projecting the polarization components on the corresponding Cartesian polarization axes results in the field distribution schematically depicted in Fig. 1(d). The linear projections of the azimuthal components on opposite sides of the intersection point are π out of phase. Together
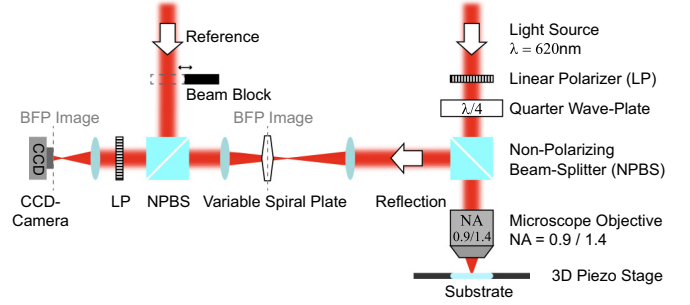
FIG. 2. Simplified sketch of the experimental setup utilized for measuring the BFP in reflection. The BFP is imaged on a variable spiral plate (VSP) in order to convert radial and azimuthal (TM and TE) field components to the x and y laboratory axes. The final linear polarizer before the CCD camera allows for selecting the intensity distribution of the desired polarization state to be recorded. In addition, the phase profile may be reconstructed via interference with a reference beam. A variation of the setup without VSP is used to directly project the polarization distribution in the BFP on Cartesian x and y axes.

with the inherent $\pm \frac{\pi}{2}$ phase delay of TE with respect to TM in CP light, a helical phase front forms around the intersection point, i.e., an optical vortex with topological charge of $\ell = \pm 1$. As a consequence, phase singularities naturally emerge in reflection in any polarization microscopy setup employing high NA.

III. SETUP

To demonstrate the emergence of a vectorial vortex beam with phase singularity in reflection at Brewster's angle, we experimentally measure the polarization state and the wavefront of the reflected light in the cylindrical polarization basis. The setup is schematically depicted in Fig. 2.

We focus a CP Gaussian beam with a wavelength of $\lambda = 620$ nm onto a BK7 glass substrate. The beam is focused tightly by a dry microscope objective of NA = 0.9 ($f_0 \approx 0.89$) or an index-matched oil immersion microscope objective of NA = 1.4 ($f_0 \approx 0.86$), used in the second part of the experiment. As mentioned earlier, the reflected field distribution in the BFP of the focusing objective is linked to the angular spectrum of the reflected focused field via the transformation in Eq. (2) [59]. Therefore, performing spatially resolved polarization and phase analysis in the BFP corresponds to an analysis of the angular spectrum of the reflected focused field. To experimentally decompose the reflected beam into its TE and TM components, we first image the objective's BFP onto a liquid-crystal-based variable spiral plate (VSP) with a topological charge of $q = 1/2$ [64], which allows for the generation of radial or azimuthal polarization patterns from incident linear polarization states and vice versa [65] (see the Appendix B). Consequently, the VSP enables us to convert the radial and azimuthal (TM and TE) field components, resulting from reflection of the focused field at the planar substrate, into the homogeneous Cartesian (x and y) laboratory axes. A combination of the VSP ($q = 1/2$) together with a subsequent linear polarizer constitutes a vector mode analyzer. The VSP converts TM (TE) into homogeneous Cartesian linear x (y)

polarization, whilst preserving the intensity and phase profile of the original TM (TE) field component. The desired polarization component is then selected by setting the transmission axis of the linear polarizer to x (y), which is explained in detail in the Appendix B. Following the geometric considerations presented in Sec. II, at θ_B only a purely azimuthally (TE) polarized vectorial vortex beam is reflected, which bears a phase singularity with topological charge of $\ell = \pm 1$. It is crucial to note here that our vector mode analyzer is mandatory only for the experimental polarization and phase characterization of the reflected light. The macroscopically large diameters d of the BFPs ($d = 3.6$ mm $\gg \lambda$ for the NA = 0.9 objective and $d = 8.9$ mm $\gg \lambda$ for the NA = 1.4 objective) allow for simply separating the emerging azimuthally polarized vortex beam by an annular aperture of suitable radius. The aperture acts as a spatial filter when placed in the BFP, selecting from the incident broad wave-vector spectrum only the waves which impinge on or emerge from the interface at Brewster's angle.

For measuring the direct projection of the reflected field on the Cartesian x and y polarization axes we remove the VSP in Fig. 2. Furthermore, interferometric measurements are performed by superposition with a reference beam possessing a planar wave front. The phase profile is successively retrieved from the recorded fringe patterns, following the procedure described by Takeda *et al.* [66].

IV. RESULTS AND DISCUSSION

The theoretically calculated and experimentally recorded intensity distributions of TE and TM polarized light in the reflection BFP of the NA = 0.9 microscope objective are depicted in Figs. 3(a)–3(d). In contrast to the TE polarized intensity, TM polarized light exhibits a prominent dark ring towards the outer edges of the BFP [67]. The different patterns originate from the distinct angular dependence of the Fresnel reflection coefficients $r^{\mathrm{TE/TM}}$, elucidated in the cross-sectional view of the incident and reflected beam's intensity alongside the evolution of $|r^{\mathrm{TE/TM}}|$ in Figs. 3(e) and 3(f). Since r^{TM} exhibits a zero crossing at Brewster's angle θ_B, a null intensity ring with corresponding radius appears in the BFP. Cropped areas of the BFP surrounding θ_B are shown as insets with enhanced contrast in Figs. 3(b) and 3(d). It must be noted that the reflected and collimated beams in the BFP of our microscope objective correspond to a superposition of paraxial modes of different orders and, therefore, change their phase front upon propagation, owing to different Gouy phases of their constituents. Consequently, for a correct phase reconstruction, we must image the BFP onto the VSP. As a result, the imperfections of the surface of the VSP are also imaged onto the camera. The central singularity of the VSP results in distortions of the experimental BFP images around the optical axis, clearly visible in Figs. 3(a) and 3(b). Next, we interfere the TE polarized field (filtered out of the beam in the BFP and converted to homogeneous Cartesian y polarization by our vector mode analyzer) with a planar phase front reference beam. A "fork" hologram with opposite orientation for incident LCP and RCP appears [see Figs. 4(a) and 4(b)], confirming the presence of a phase vortex with topological charge of $\ell = \pm 1$. The corresponding reconstructed experi-
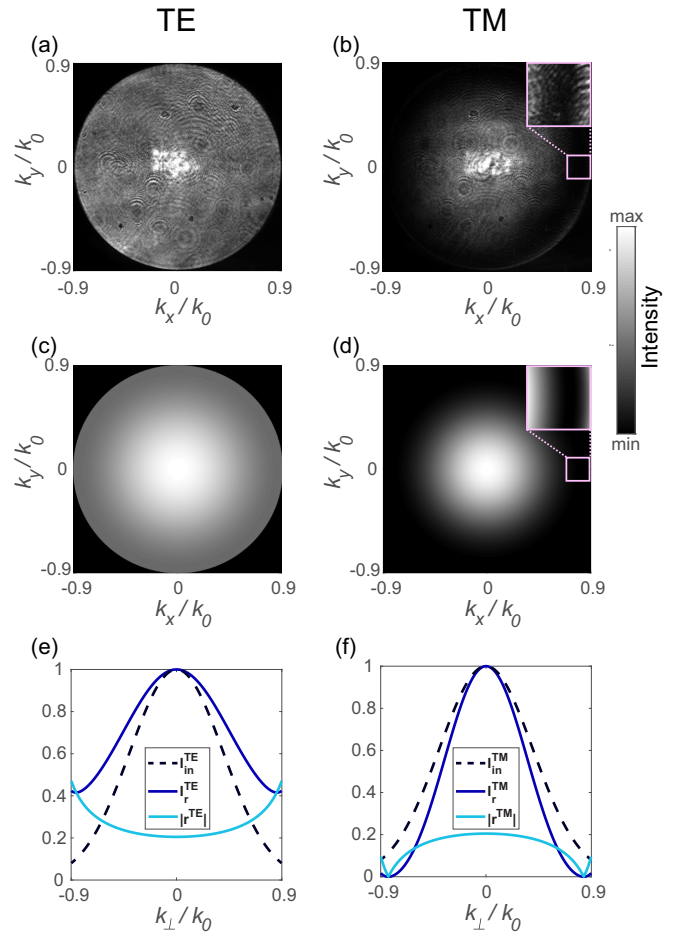
FIG. 3. (a, b) Experimental and (c, d) theoretical intensity distributions in the BFP of the NA = 0.9 microscope objective, for reflection of a focused CP Gaussian beam from a BK7 glass substrate. In contrast to the rather homogeneous intensity distribution for TE polarized light (a, c), the projection on TM (b, d) shows a null intensity ring with radius corresponding to Brewster's angle θ_B. The insets in panels (b) and (d) show cropped areas of the BFP surrounding θ_B with enhanced contrast. (e, f) Cross-sectional view of the calculated TE and TM projections for the incident and reflected beam's intensity distributions I_{in} and I_r (normalized to their respective maximum), alongside the absolute value of the corresponding Fresnel reflection coefficient $|r^{\mathrm{TE/TM}}|$.

mental and theoretical phases are shown in Figs. 4(c) and 4(d) and Figs. 4(e) and 4(f), respectively. The phase images validate the natural emergence of a vectorial vortex beam with central phase singularity in the surprisingly common configuration of focused CP light, reflected from a dielectric substrate at Brewster's angle θ_B. It must be noted, however, that a decomposition of a CP beam into TE and TM components introduces phase singularities with topological charge of $\ell = \pm 1$ (see Sec. II and Appendix A). Therefore, the mentioned azimuthally polarized vectorial vortex beam presented in Fig. 4 appears only at the angular range corresponding to Brewster's angle (vanishing TM component), which manifests itself as a dark ring in Figs. 3(b) and 3(d).

A frequently applied scheme in polarization microscopy utilizes index-matched immersion oil in the focusing path for
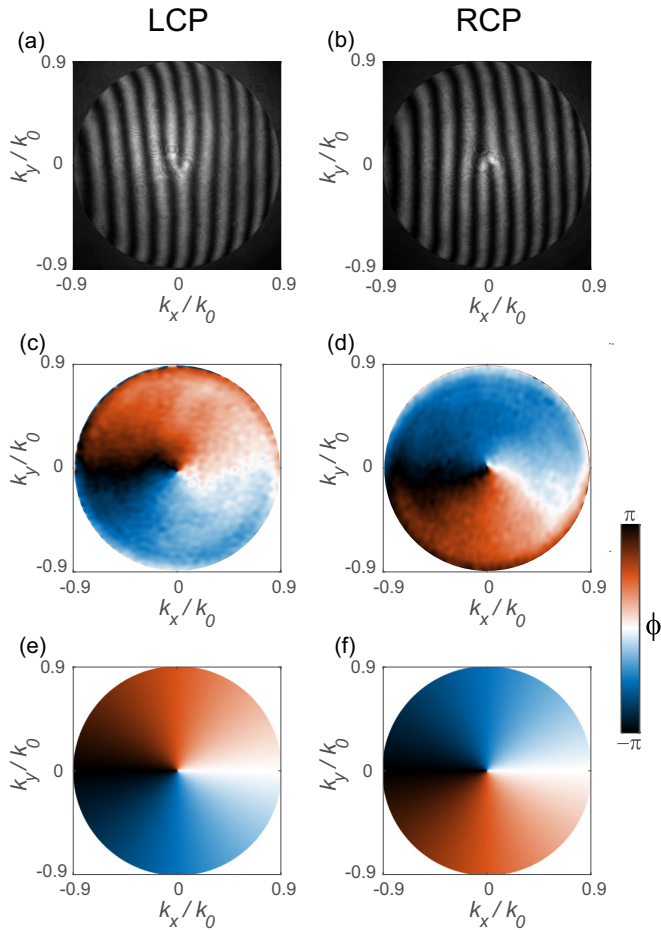
FIG. 4. (a, b) Interference patterns of TE polarized reflected light with a planar-wavefront reference beam for incident left- and right-hand CP (LCP and RCP) in the BFP of the NA = 0.9 microscope objective, displaying fork holograms of opposite orientations. (c, d) Corresponding experimental and (e, f) theoretical phase fronts, verifying the presence of a central singularity surrounded by a helical phase distribution.

FIG. 5. (a, b) Experimental and (c, d) theoretical intensity distributions in the BFP of the NA = 1.4 oil immersion microscope objective, for reflection of a focused CP Gaussian beam from the glass-air interface at the bottom of a BK7 substrate. As for the case with the dry NA = 0.9 objective in Fig. 3, a null intensity ring at Brewster's angle θ_B shows up for TM polarized light (b, d), contrary to the projection on TE polarization (a, c). Furthermore, the sharp transition at the critical angle for total internal reflection θ_c and the high intensity above it are prominent in all images. (e, f) Cross-sectional view of the calculated TE and TM projections for the incident and reflected beam's intensity distributions I_{in} and I_r (normalized to their respective maximum), alongside the absolute value of the corresponding Fresnel reflection coefficient $|r^{TE/TM}|$.

investigation of specimens on a substrate in a homogeneous environment. Since Brewster's angle also appears for the transition to an optically denser medium, e.g., glass to air, similar effects are observed in this measurement scheme. We present corresponding results in Fig. 5, using an index-matched oil immersion objective of NA = 1.4. We benefit from this scheme not only by a broader range of incidence angles, but also by total internal reflection above the critical angle θ_c, which due to its vicinity to θ_B increases the visibility of the dark ring at Brewster's angle for TM polarization. As shown in Fig. 5, the theoretical and experimental intensity distributions for TE and TM nicely reproduce the expected features. Apart from the dark Brewster ring in the TM projection of the BFP, the sharp transition at the critical angle as well as the high intensity above it are evident for both polarizations.

In the next step, we show that Brewster's effect leads to the emergence of phase vortices even in the ubiquitous case of a polarization projection onto Cartesian axes. Therefore, we remove the VSP (see Fig. 2), resulting in a projection of the reflected beam onto Cartesian x and y instead of cylindrical TM

and TE coordinates by the final linear polarizer. As discussed in Sec. II, for a projection of the BFP polarization distribution onto x and y, we expect two phase vortices forming at the intersection points of the Brewster ring and the respective Cartesian axis. Indeed, the interference patterns for incident RCP in Figs. 6(a) and 6(b) clearly show the emergence of two horizontally or vertically aligned forks at θ_B, depending on the Cartesian axis chosen for projection. Likewise, phase reconstruction around both points corroborates the expectation of vortices with topological charge of $\ell = \pm 1$, as shown in the helical phase profiles in Figs. 6(c) and 6(d). As a result, the presence of these parasitic phase singularities must be considered for any linear polarization projection in reflection from focusing geometries covering Brewster's angle.
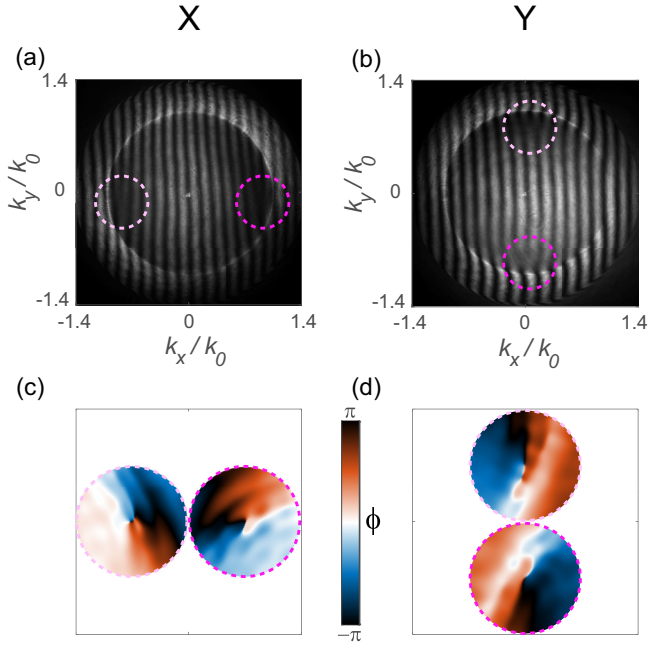
FIG. 6. (a, b) Interference patterns of x and y polarized projections of the reflected light with a planar-wavefront reference beam for incident RCP in the BFP of the NA = 1.4 microscope objective. Two horizontally (x) or vertically (y) aligned forks emerge at the intersection points of the Brewster ring and respective Cartesian axis. (c, d) Phase reconstruction around these points affirms the presence of vortices with topological charge of $\ell = \pm 1$.

V. CONCLUSION

In conclusion, we experimentally demonstrated the inevitable emergence of phase singularities and generation of vectorial vortices upon reflection of focused CP light from a dielectric substrate under Brewster's angle. Specifically, we utilized a variable spiral plate with a topological charge of $q = 1/2$ to separate the TE and TM polarized field components of the reflected CP Gaussian input beam and directly demonstrated the emergence of an azimuthally polarized vectorial vortex beam with a phase singularity, appearing at Brewster's angle. Additionally, we performed interferometry in reflection to directly reconstruct the phase profile in the BFP. Moreover, we also demonstrated and interpreted the presence of phase singularities for an even simpler measurement scheme, performing a polarization projection of the reflected field distribution in the BFP onto Cartesian axes.

The utilized experimental scheme is so common, especially in the field of polarization microscopy, that our findings have to be considered widely wherever high NA focusing geometries for phase and polarization sensitive measurements in reflection are employed. Furthermore, our paper provides an experimentally and conceptually straightforward basis for generation of vectorial vortex beams with a phase singularity, which are of great interest in a broad range of applications utilizing exotic states of light.

APPENDIX A: POLARIZATION BASIS

First, we define the polarization basis using Dirac bra-ket notation. Starting with homogeneous horizontal $\mathbf{e}_x \equiv |x\rangle$ and vertical $\mathbf{e}_y \equiv |y\rangle$ polarizations, we construct the LCP and RCP $\mathbf{e}_\pm \equiv |\pm\rangle$ states. The space variant cylindrical radial $\mathbf{e}_\rho \equiv |\rho\rangle$ and azimuthal $\mathbf{e}_\phi \equiv |\phi\rangle$ polarization vectors depend on the angle ϕ at the specific location in the transverse xy plane. We summarize this transformation as follows:

$$|+\rangle = \frac{1}{\sqrt{2}}(|x\rangle + \iota|y\rangle),$$

$$|-\rangle = \frac{1}{\sqrt{2}}(|x\rangle - \iota|y\rangle),$$

$$|\rho\rangle = +\cos\phi|x\rangle + \sin\phi|y\rangle,$$

$$|\phi\rangle = -\sin\phi|x\rangle + \cos\phi|y\rangle. \tag{A1}$$

We use the representation in Eqs. (A1) to show the emergence of a helical phase front $\propto \exp(\pm\iota\phi)$ upon projection of circular polarizations $|\pm\rangle$ onto $|\phi\rangle$ and $|\rho\rangle$:

$$\langle\phi|\pm\rangle = \frac{\pm\iota}{\sqrt{2}}(\cos\phi \pm \iota\sin\phi) = \frac{\pm\iota}{\sqrt{2}}\exp(\pm\iota\phi),$$

$$\langle\rho|\pm\rangle = \frac{1}{\sqrt{2}}(\cos\phi \pm \iota\sin\phi) = \frac{1}{\sqrt{2}}\exp(\pm\iota\phi). \tag{A2}$$

We also list the projections of cylindrical polarization vectors on Cartesian ones and vice versa, which become useful later:

$$\langle\rho|x\rangle = \langle x|\rho\rangle = +\cos\phi,$$

$$\langle\rho|y\rangle = \langle y|\rho\rangle = +\sin\phi,$$

$$\langle\phi|x\rangle = \langle x|\phi\rangle = -\sin\phi,$$

$$\langle\phi|y\rangle = \langle y|\phi\rangle = +\cos\phi, \tag{A3}$$

where we drop the complex conjugate of the term in the middle of each equation, since all quantities appearing in Eqs. (A3) are real.

APPENDIX B: VECTOR MODE ANALYZER

The action of a VSP with a topological charge of q on the optical field at each point of the transverse plane xy consists of rotation of the polarization vector by an angle of $2q\phi$ with respect to the x axis (assumed to be the axis of the VSP) [24,64,65]. Consequently, a VSP with a topological charge of $q = 1/2$ converts incident $|x\rangle$ and $|y\rangle$ polarizations to $+|\rho\rangle$ and $-|\phi\rangle$, respectively, and its Jones matrix can be written as [24]

$$\hat{q}_{1/2} = |\rho\rangle\langle x| - |\phi\rangle\langle y|. \tag{B1}$$

It is straightforward to see from Eqs. (A3) and (B1) that $\hat{q}_{1/2}$ is Hermitian and unitary $\hat{q}_{1/2} = \hat{q}_{1/2}^* = \hat{q}_{1/2}^{-1}$, which allows us to derive the action of the VSP on a cylindrical polarization basis:

$$\hat{q}_{1/2} = \hat{q}_{1/2}^{-1} = \hat{q}_{1/2}^* = |x\rangle\langle\rho| - |y\rangle\langle\phi|. \tag{B2}$$

We can directly verify the result in Eq. (B2) by sandwiching $\hat{q}_{1/2}$ in Eq. (B1) between two unity operators $\hat{I}_{(x,y)}$ and $\hat{I}_{(\rho,\phi)}$ and using the relations in Eqs. (A3):

$$\hat{I}_{(x,y)} = |x\rangle\langle x| + |y\rangle\langle y|,$$

$$\hat{I}_{(\rho,\phi)} = |\rho\rangle\langle\rho| + |\phi\rangle\langle\phi|,$$

$$\hat{q}_{1/2} = \hat{I}_{(x,y)}\hat{q}_{1/2}\hat{I}_{(\rho,\phi)} = |x\rangle\langle\rho| - |y\rangle\langle\phi|. \quad \text{(B3)}$$

A linear polarizer acting on the field after the VSP can be represented as a projection operator $\hat{P}$, and the combination of both yields

$$\hat{P}_x = |x\rangle\langle x|, \quad \hat{P}_y = |y\rangle\langle y|,$$

$$\hat{P}_x\hat{q}_{1/2} = +|x\rangle\langle\rho|, \quad \hat{P}_y\hat{q}_{1/2} = -|y\rangle\langle\phi|. \quad \text{(B4)}$$

Equations (B4) are the cornerstone of our experimental analysis. They show that a combination of a VSP with a topological charge of $q = 1/2$ and a linear polarizer (analyzer) acts as a vector mode analyzer [68]. Moreover, incident radial and azimuthal polarizations are converted to homogeneous Cartesian x and y polarizations, respectively, without any distortion in their intensity and phase profiles (up to a global factor) [69,70]. This property of our vector mode analyzer allows for direct reconstruction of intensity and phase profiles of radial and azimuthal components of the beam. To reconstruct the phase profile, we set the linear analyzer to x (y) and interfere the transmitted beam with a linearly x (y) polarized reference beam with a planar wavefront. The obtained fork hologram [66] represents the phase of the radial (azimuthal) component of the incident beam, as shown in Fig. 4.

[1] M. Born and E. Wolf, *Principles of Optics: Electromagnetic Theory of Propagation, Interference and Diffraction of Light* (Elsevier, Amsterdam, 2013).

[2] H. Rubinsztein-Dunlop, A. Forbes, M. V. Berry, M. R. Dennis, D. L. Andrews, M. Mansuripur, C. Denz, C. Alpmann, P. Banzer, T. Bauer, E. Karimi, L. Marrucci, M. Padgett, M. Ritsch-Marte, N. M. Litchinitser, N. P. Bigelow, C. Rosales-Guzmán, A. Belmonte, J. P. Torres, T. W. Neely, M. Baker, R. Gordon, A. B. Stilgoe, J. Romero, A. G. White, R. Fickler, A. E. Willner, G. Xie, B. McMorran, and A. M. Weiner, J. Opt. **19**, 013001 (2017).

[3] Q. Zhan, Adv. Opt. Photon. **1**, 1 (2009).

[4] Q. Zhan and J. R. Leger, Opt. Express **10**, 324 (2002).

[5] V. G. Niziev and A. V. Nesterov, J. Phys. D **32**, 1455 (1999).

[6] R. Dorn, S. Quabis, and G. Leuchs, Phys. Rev. Lett. **91**, 233901 (2003).

[7] M. Neugebauer, P. Woźniak, A. Bag, G. Leuchs, and P. Banzer, Nat. Commun. **7**, 11286 (2016).

[8] A. Bag, M. Neugebauer, P. Woźniak, G. Leuchs, and P. Banzer, Phys. Rev. Lett. **121**, 193902 (2018).

[9] L. Allen, M. W. Beijersbergen, R. J. C. Spreeuw, and J. P. Woerdman, Phys. Rev. A **45**, 8185 (1992).

[10] A. T. O'Neil, I. MacVicar, L. Allen, and M. J. Padgett, Phys. Rev. Lett. **88**, 053601 (2002).

[11] A. M. Yao and M. J. Padgett, Adv. Opt. Photon. **3**, 161 (2011).

[12] K. Y. Bliokh, M. A. Alonso, E. A. Ostrovskaya, and A. Aiello, Phys. Rev. A **82**, 063825 (2010).

[13] K. Y. Bliokh and F. Nori, Phys. Rep. **592**, 1 (2015).

[14] S. Franke-Arnold, L. Allen, and M. Padgett, Laser Photon. Rev. **2**, 299 (2008).

[15] K. Y. Bliokh, F. J. Rodríguez-Fortuño, F. Nori, and A. V. Zayats, Nat. Photon. **9**, 796 (2015).

[16] H. He, M. E. J. Friese, N. R. Heckenberg, and H. Rubinsztein-Dunlop, Phys. Rev. Lett. **75**, 826 (1995).

[17] M. Stütz, S. Gröblacher, T. Jennewein, and A. Zeilinger, Appl. Phys. Lett. **90**, 261114 (2007).

[18] S. W. Hell, Nat. Biotechnol. **21**, 1347 (2003).

[19] M. Ritsch-Marte, Philos. Trans. R. Soc. A **375**, 20150437 (2017).

[20] G. Biener, A. Niv, V. Kleiner, and E. Hasman, Opt. Lett. **27**, 1875 (2002).

[21] Z. Bomzon, G. Biener, V. Kleiner, and E. Hasman, Opt. Lett. **27**, 1141 (2002).

[22] K. Y. Bliokh, E. A. Ostrovskaya, M. A. Alonso, O. G. Rodríguez-Herrera, D. Lara, and C. Dainty, Opt. Express **19**, 26132 (2011).

[23] L. Marrucci, C. Manzo, and D. Paparo, Phys. Rev. Lett. **96**, 163905 (2006).

[24] L. Marrucci, E. Karimi, S. Slussarenko, B. Piccirillo, E. Santamato, E. Nagali, and F. Sciarrino, J. Opt. **13**, 064001 (2011).

[25] E. Brasselet, N. Murazawa, H. Misawa, and S. Juodkazis, Phys. Rev. Lett. **103**, 103903 (2009).

[26] Y. Gorodetski, S. Nechayev, V. Kleiner, and E. Hasman, Phys. Rev. B **82**, 125433 (2010).

[27] E. Karimi, S. A. Schulz, I. De Leon, H. Qassim, J. Upham, and R. W. Boyd, Light: Sci. Appl. **3**, e167 (2014).

[28] D. Garoli, P. Zilio, Y. Gorodetski, F. Tantussi, and F. De Angelis, Sci. Rep. **6**, 29547 (2016).

[29] N. Shitrit, I. Yulevich, E. Maguid, D. Ozeri, D. Veksler, V. Kleiner, and E. Hasman, Science **340**, 724 (2013).

[30] J. Lin, J. P. B. Mueller, Q. Wang, G. Yuan, N. Antoniou, X.-C. Yuan, and F. Capasso, Science **340**, 331 (2013).

[31] A. Ciattoni, G. Cincotti, and C. Palma, Phys. Rev. E **67**, 036618 (2003).

[32] A. Ciattoni, G. Cincotti, and C. Palma, J. Opt. Soc. Am. A **20**, 163 (2003).

[33] A. Volyar, V. Shvedov, T. Fadeyeva, A. S. Desyatnikov, D. N. Neshev, W. Krolikowski, and Y. S. Kivshar, Opt. Express **14**, 3724 (2006).

[34] E. Brasselet, Y. Izdebskaya, V. Shvedov, A. S. Desyatnikov, W. Krolikowski, and Y. S. Kivshar, Opt. Lett. **34**, 1021 (2009).

[35] M. G. Nassiri and E. Brasselet, Phys. Rev. A **99**, 013836 (2019).

[36] D. Fink, Appl. Opt. **18**, 581 (1979).

[37] T. Wakayama, K. Komaki, Y. Otani, and T. Yoshizawa, Opt. Express **20**, 29260 (2012).

[38] T. Wakayama, O. G. Rodríguez-Herrera, J. S. Tyo, Y. Otani, M. Yonemura, and T. Yoshizawa, Opt. Express **22**, 3306 (2014).

[39] J.-F. Bisson, J. Li, K. Ueda, and Y. Senatsky, Opt. Express **14**, 3304 (2006).

[40] M. Mansuripur, A. R. Zakharian, and E. M. Wright, Phys. Rev. A **84**, 033813 (2011).

[41] H. Kobayashi, K. Nonaka, and M. Kitano, Opt. Express **20**, 14064 (2012).

[42] F. Bouchard, H. Mand, M. Mirhosseini, E. Karimi, and R. W. Boyd, New J. Phys. **16**, 123006 (2014).

[43] A. Aleksanyan and E. Brasselet, Optica **3**, 167 (2016).

[44] N. Radwell, R. Hawley, J. B. Götte, and S. Franke-Arnold, Nat. Commun. **7**, 10564 (2016).

[45] Y. Zhao, J. S. Edgar, G. D. M. Jeffries, D. McGloin, and D. T. Chiu, Phys. Rev. Lett. **99**, 073901 (2007).

[46] I. Fernandez-Corbaton, X. Zambrana-Puyalto, and G. Molina-Terriza, Phys. Rev. A **86**, 042103 (2012).

[47] I. Fernandez-Corbaton, X. Zambrana-Puyalto, N. Tischler, X. Vidal, M. L. Juan, and G. Molina-Terriza, Phys. Rev. Lett. **111**, 060401 (2013).

[48] L. Novotny, R. D. Grober, and K. Karrai, Opt. Lett. **26**, 789 (2001).

[49] W. Nasalski, Opt. Commun. **197**, 217 (2001).

[50] W. Nasalski, Phys. Rev. E **74**, 056613 (2006).

[51] W. Nasalski and Y. Pagani, J. Opt. A **8**, 21 (2006).

[52] M. Yavorsky and E. Brasselet, Opt. Lett. **37**, 3810 (2012).

[53] A. Ciattoni, A. Marini, and C. Rizza, Phys. Rev. Lett. **118**, 104301 (2017).

[54] D. Brewster, Proc. R. Soc. A **2**, 14 (1815).

[55] R. Paniagua-Domínguez, Y. F. Yu, A. E. Miroshnichenko, L. A. Krivitsky, Y. H. Fu, V. Valuckas, L. Gonzaga, Y. T. Toh, A. Y. S. Kay, B. Luk'yanchuk *et al.*, Nat. Commun. **7**, 10362 (2016).

[56] H. Luo, X. Zhou, W. Shu, S. Wen, and D. Fan, Phys. Rev. A **84**, 043806 (2011).

[57] L.-J. Kong, X.-L. Wang, S.-M. Li, Y. Li, J. Chen, B. Gu, and H.-T. Wang, Appl. Phys. Lett. **100**, 071109 (2012).

[58] A. Aiello, M. Merano, and J. P. Woerdman, Opt. Lett. **34**, 1207 (2009).

[59] L. Novotny and B. Hecht, *Principles of Nano-Optics* (Cambridge University Press, Cambridge, England, 2012).

[60] D. S. Citrin, Opt. Lett. **37**, 2376 (2012).

[61] S. A. Empedocles, R. Neuhauser, and M. G. Bawendi, Nature (London) **399**, 126 (1999).

[62] C. Sönnichsen and A. P. Alivisatos, Nano Lett. **5**, 301 (2005).

[63] P. Whittaker, R. A. Kloner, D. R. Boughner, and J. G. Pickering, Basic Res. Cardiol. **89**, 397 (1994).

[64] S. Slussarenko, A. Murauski, T. Du, V. Chigrinov, L. Marrucci, and E. Santamato, Opt. Express **19**, 4085 (2011).

[65] F. Cardano, E. Karimi, S. Slussarenko, L. Marrucci, C. de Lisio, and E. Santamato, Appl. Opt. **51**, C1 (2012).

[66] M. Takeda, H. Ina, and S. Kobayashi, J. Opt. Soc. Am. **72**, 156 (1982).

[67] G. López-Morales, V.-M. Rico-Botero, R. Espinosa-Luna, and Q. Zhan, Chin. Opt. Lett. **15**, 030004 (2017).

[68] S. Nechayev, J. S. Eismann, M. Neugebauer, P. Woźniak, A. Bag, G. Leuchs, and P. Banzer, Phys. Rev. A **99**, 041801(R) (2019).

[69] S. Nechayev, M. Neugebauer, M. Vorndran, G. Leuchs, and P. Banzer, Phys. Rev. Lett. **121**, 243903 (2018).

[70] M. Neugebauer, S. Nechayev, M. Vorndran, G. Leuchs, and P. Banzer, Nano Lett. **19**, 422 (2019).